Available online at www.sciencedirect.com
SCIENCE DIRECT®
Journal of the European Ceramic Society 25 (2005) 1241–1249
www.elsevier.com/locate/jeurceramsoc

Fracture characteristics of Al_2O_3/YAG composite at room temperature to 2023 K

S. Ochiai[a,*], Y. Sakai[b], K. Sato[b], M. Tanaka[b], M. Hojo[b], H. Okuda[a], Y. Waku[c], N. Nakagawa[c], S. Sakata[c], A. Mitani[c], T. Takahashi[d]

[a] *Division of Research Initiatives, International Innovation Center, Kyoto University, Sakyo-ku, Kyoto 606-8501, Japan*
[b] *Graduate School of Engineering, Kyoto University, Sakyo-ku, Kyoto 606-8501, Japan*
[c] *Ube Research Laboratory, Corporate Research and Development, UBE Industries Ltd., 1978-5 Kogushi, Ube, Yamaguchi 755-8633, Japan*
[d] *Ube Scientific Analysis Laboratory, Inc., 1978-5 Kogushi, Ube, Yamaguchi 755-8633, Japan*

Available online 26 January 2005

Abstract

The fracture behavior of the notched unidirectionally solidified eutectic Al_2O_3/YAG composite was investigated by tensile test at room temperature to 2023 K, and the results were analyzed by the finite element method. The stress–strain behavior, notched strength and the fracture toughness were strongly dependent on temperature and displacement speed. The specimens fractured in a brittle manner at low temperatures and at high displacement speeds but in a ductile manner accompanying plastic deformation at high temperatures and at low displacement speeds. The notched strength for a given displacement speed of 10^{-7} m/s increased with increasing temperature from 132 MPa at 1873 K to 153 MPa at 1923 K, and then decreased to 133 and 110 MPa at 1973 and 2023 K, respectively. Also the notched strength for a given temperature of 2023 K increased with decreasing displacement speed from 67 MPa at the displacement speed of 10^{-5} m/s to 124 MPa at 10^{-6} m/s, and then decreased to 110 and 72 MPa at 10^{-7} and 10^{-8} m/s, respectively. The stress distribution and the plastic zone size ahead of the notch were calculated by a finite element method using the dependence of flow stress on temperature and displacement speed. Based on the calculation result, the experimentally observed increase in the notched strength with increasing temperature and decreasing displacement speed up to the maximum value could be accounted for by the increase in plastic zone size ahead of the notch. Also, the observed decrease in notched strength with further increasing temperature and decreasing displacement speed could be accounted for by the decrease in the stress carrying capacity of the yielded ligament.

Keywords: Al_2O_3/YAG; Composite; Failure analysis; Mechanical properties; Strength

1. Introduction

Directionally solidified eutectic ceramic composites have clean interface, high thermodynamical-compatibility between/among the constituting phases, and high static and creep strengths, as has been reported by many researchers based on the microstructural, crystallographic and mechanical studies.[1–25] Among many eutectic composites, oxide/oxide systems such as $Al_2O_3/ZrO_2(Y_2O_3)$,[3–5,18–20,23] $Al_2O_3/Y_3Al_{15}O_{12}$(YAG),[6–9,11–15,21,22] $Al_2O_3/Er_3Al_5O_{12}$[16,26] and $Al_2O_3/GdAlO_3$[10,25] are promising for high temperature use as fiber materials for reinforcement and as bulk materials for machine parts due to high oxidation-resistance.

Concerning the bulk-type Al_2O_3/YAG, $Al_2O_3/Er_3Al_5O_{12}$ and $Al_2O_3/GdAlO_3$ eutectic composites prepared at Ultra High Temperature Materials Research Center, Yamaguchi, Japan, the following features have been reported by Waku et al.[6–8,10–12], Yoshida et al.[15], Nakagawa et al.[16] and Ochiai et al.[21] (a) They consist of continuous networks of single crystal ⟨1 1 0⟩ Al_2O_3 and single crystal ⟨1 1 0⟩ YAG ($Er_3Al_5O_{12}$, $GdAlO_3$)[6–8,10–12,16] and the interface is clean without grain boundary and glassy phase.[6,8,10,11,16] (b) The microstructure is very stable. For instance, even after the exposure in air at 1973 K for 1000 h, it is same as before.[6]

* Corresponding author. Tel.: +81 75 753 4834; fax: +81 75 753 4841.
E-mail address: ochicai@mech.kyoto-u.ac.jp (S. Ochiai).

0955-2219/$ – see front matter © 2005 Elsevier Ltd. All rights reserved.
doi:10.1016/j.jeurceramsoc.2005.01.006

(c) The bending strength of Al_2O_3/YAG at room temperature, around 400 MPa, can be maintained almost up to the melting point of 2093 K when the displacement speed is high.[6–8,15,21] The bending yield stress of $Al_2O_3/GdAlO_3$ is so high as around 700 MPa at 1873 K.[10] (d) Compressive creep strength at 1873 K is about 13 times higher than that of the sintered composite with the same composition.[8,12] Due to these excellent stability of microstructure and mechanical property at ultra high temperatures, the maximum operating temperature of these composites can be 1773–1973 K, being much higher than that (1323–1373 K) of Ni-based single crystal cast superalloys and that (~1300 K) of oxide ceramics.[6,10] Therefore, several useful applications can be considered, for instance, gas turbines and power-generation systems with non-cooled turbine blades at very high temperatures.[10]

For practical application of these composites, it is requested to accumulate experimental data and to reveal the mechanism of deformation and fracture. In our former work,[21] the deformation and fracture behavior of the unnotched and notched bulk-type Al_2O_3/YAG composite specimens was investigated by bending test at room temperature to 2023 K under various displacement speeds. Following features were observed.

(A) The load–displacement curve of unnotched specimens was dependent on the test temperature and displacement speed, as shown in Fig. 1(a)–(c). Below 1773 K, the specimens were brittle at all displacement speeds investigated. Beyond 1823 K, the ductility was dependent on the displacement speed. At the low displacement speed of 8.3×10^{-8} m/s (a), the specimens were ductile from 1823 to 2023 K. At 8.3×10^{-7} m/s (b), the ductility was lost at 1823 K while it was kept in the temperature range from 1873 to 2023 K. At the high speed of 8.3×10^{-6} (c), the specimens were brittle at all temperatures investigated. In this way, the unnotched specimens fractured in a brittle manner at low temperatures and at high displacement speeds but in a ductile manner accompanying plastic deformation at high temperatures and at low displacement speed. Correspondingly, the brittle–ductile transition temperature increased with increasing displacement speed.

(B) At the lower displacement speeds of 8.3×10^{-7} m/s and 8.3×10^{-8} m/s, the unnotched strength of the specimens, which fractured in a ductile manner, decreased with increasing temperature (Fig. 1(a′) and (b′)). At the higher displacement speed of 8.3×10^{-6} m/s, at which all specimens fractured in a brittle manner, the strength

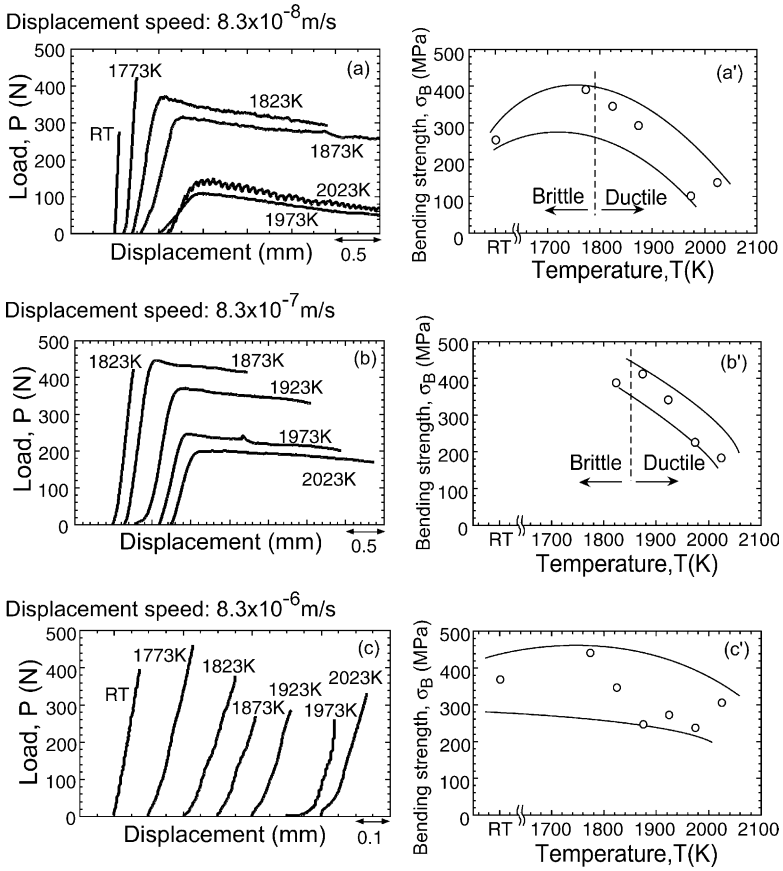

Fig. 1. (a, b, c) Load–displacement curve and (a′, b′, c′) strength of unnotched specimens measured by the three-point bending test at room temperature to 2023 K at the displacement speeds of (a, a′) 8.3×10^{-8}, (b, b′) 8.3×10^{-7} m/s and (c, c′) 8.3×10^{-6} m/s.

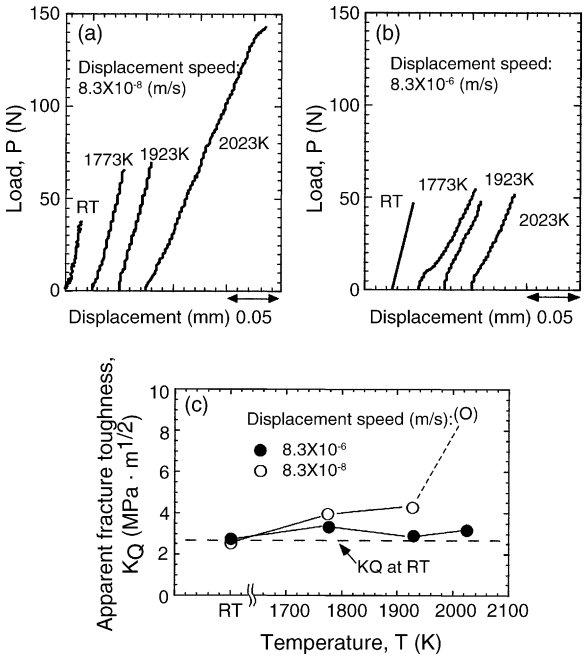

Fig. 2. Load–displacement curves of the notched specimens measured by the three-point bending test at room temperature to 2023 K at the displacement speeds of (a) 8.3×10^{-8} m/s and (b) 8.3×10^{-6} m/s, and the change of apparent mode I fracture toughness with increasing temperature (c).

value at room temperature was almost maintained up to 2023 K (Fig. 1(c′)).

(C) The dependence of load–displacement curve and fracture toughness of notched specimens on temperature and displacement speed is shown in Fig. 2. When the displacement speed was low (8.3×10^{-8} m/s), the notched strength increased with increasing temperature (Fig. 2(a)). On the contrary, when the displacement speed was high (8.3×10^{-6} m/s), the strength was nearly the same at any temperature (Fig. 2(b)). Accordingly, the apparent fracture toughness value K_Q, estimated by the linear elastic fracture mechanics, was nearly constant for 8.3×10^{-6} m/s but it increased with increasing temperature for 8.3×10^{-8} m/s, as shown in Fig. 2(c). The K_Q value of the specimen tested at the displacement speed of 8.3×10^{-8}m/s at 2023 K is shown in the parentheses for reference since the application of the linear elastic fracture mechanics might be limited due to the enhanced plastic zone ahead of the notch.

These results indicate that the plastic zone formation ahead of the notch, which plays a dominant role for determination of the K_Q value, is dependent on displacement speed and temperature. Considering the temperature and displacement speed dependence of the growth of plastic zone, the following behavior can be expected.

(i) When the plastic flow takes place ahead of the notch, it acts to raise the notched strength. As the plastic flow stress decreases and therefore the plastic zone size increases with increasing temperature, the notched strength (and fracture toughness) is expected to increase with increasing temperature. On the other hand, as the flow stress decreases with further increasing temperature, the plastic zone ahead of the notch can be large enough to cover the ligament in the notched cross-section (overall yielding). At such high temperatures, the notch extension is suppressed due to the enhanced plastic deformation but the flow stress decreases with increasing temperature, resulting in decrease in the stress carrying capacity of the ligament. As a result, the strength of notched specimens decreases with increasing temperature. Thus, it is expected that, for a given displacement speed, the notched strength increases and then decreases with increasing temperature.

(ii) At very high temperatures, the composite is ductile at low displacement speeds, while it is brittle at low speeds. At low displacement speed range, the plastic zone grows to cover the ligament, and the notch extension is suppressed. In such a situation, the stress carrying capacity of the ligament and therefore the strength of notched specimens increase with increasing displacement speed due to the increasing flow stress. On the other hand, at high displacement speed range where overall yielding of ligament does not take place, the size of the plastic zone ahead of the notch is limited and the specimen fractures in a brittle manner. In such a situation, as the flow stress increases with increasing displacement speed, the size of the plastic zone and therefore the notched strength decrease with increasing displacement speed. Thus, it is expected that the notched strength increases but then decreases with increasing displacement speed.

In this way, it is expected that, under a given displacement speed, the notched strength increases with increasing temperature, reaching maximum and then decreases. Similarly, it is expected that, under a given temperature, it increases with increasing displacement speed, reaching maximum and then decreases. The aims of the present work are (1) to examine experimentally whether the expected feature appears or not by tensile test of the notched bulk-type Al_2O_3/YAG composite specimens at 1873 to 2023 K, and (2) to describe the temperature and displacement speed dependence of the notched strength from the viewpoint of the stress and plastic zone distributions by means of the finite element analysis.

2. Experimental procedure

2.1. Specimens and test method

The commercially available α-Al_2O_3 powders with the purity higher than 99.99 mass% (AKP-30, produced by Sumitomo Chemical Co. Ltd.) and Y_2O_3 powders with the purity higher than 99.9 mass% (Y_2O_3-RU, submicron-type, produced by Shin-etsu Chemical Co. Ltd.) were mixed in the eutectic molar ratio of 82:18. The mixed powders were

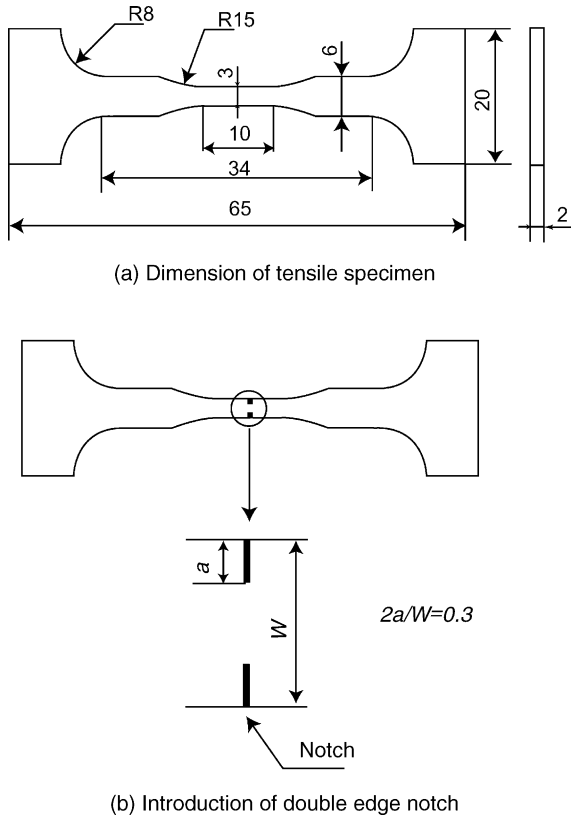

Fig. 3. Schematic representation of the notched specimens for tensile test. (a) Dimension in mm. (b) Configuration of double edge notch.

ball-milled in ethanol to achieve high homogeneity. The obtained slurry was dried and pre-melt by arc melting to obtain initial ingots. The ingots were crushed and the resultant powders were molten in a Mo crucible by high frequency induction heating at a pressure of 1.3×10^{-3} Pa in an argon atmosphere. After the melt was sustained at 2223 K for 1.8 ks, it was solidified unidirectionally by descending the Mo crucible at a speed of 1.39×10^{-6} m/s under the atmosphere stated above. The temperature gradient at the liquid–solid interface was approximately 8 K/cm.

Tensile test was carried out for the double edge notched specimens shown in Fig. 3 using the high temperature testing system (Instron type 8562) at Japan Ultra High Temperature Materials Research Center. The notch-tip radius was made 50 μm with a special saw. The relative notch length ($2a/W$ where a and W are the notch length and specimen width, respectively) was 0.3. The specimens were heated to the prescribed temperatures under an argon atmosphere, held for 5 min and then tested. The test was carried out at the temperatures of 1873, 1923, 1973 and 2023 K under the displacement speed of 10^{-7} m/s and at the displacement speeds of 10^{-8}, 10^{-7}, 10^{-6} and 10^{-5} m/s under the temperature of 2023 K.

The notched specimens showed brittle and ductile fracture modes depending on test temperature and displacement speed as will be shown later in Section 3.1. For the specimens that fractured in a brittle mode, the apparent fracture toughness

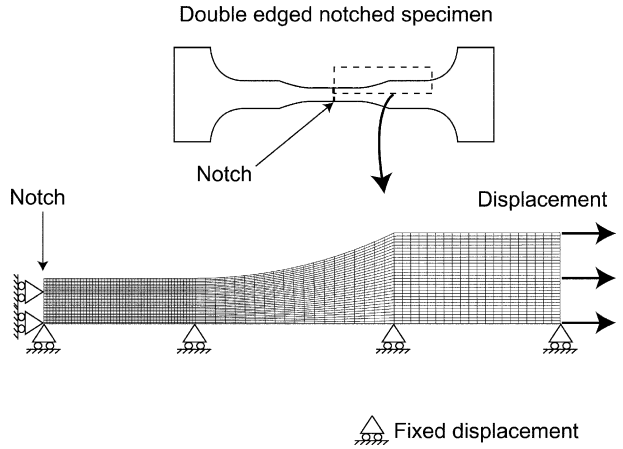

Fig. 4. Employed meshes and boundary conditions for the finite element analysis.

K_Q was estimated by:[27]

$$K_Q = \sigma_N(\pi a)^{1/2} F(\xi) \quad (1)$$

$$F(\xi) = \frac{(1.122 - 0.56\xi - 0.205\xi^2 + 0.471\xi^3 - 0.190\xi^4)}{(1-\xi)^{1/2}} \quad (\xi = 2a/W) \quad (2)$$

where σ_N is the notched strength, estimated by dividing the ultimate load by the gross cross-sectional area.

2.2. Finite element analysis

The finite element analysis for notched tensile specimens was carried out with the commercial finite element code MARC/Mentat™. The employed meshes and boundary conditions are presented in Fig. 4. The analysis was carried out under the plane strain condition. For calculation of the stress state of unnotched specimens, the notch was removed under the same meshes and boundary conditions.

The temperature (T) dependence of the Young's modulus of the composite (E_c) was taken from our former work,[28] $E_c = 356 - 0.0310T$ (GPa). The Poisson's ratio, ν_c, of the composite was taken to be 0.24, since the Poisson's ratios of Al_2O_3 and YAG are 0.23 and 0.25, respectively[29] and the volume fraction of each phase is 0.5.[6–8,11,12,15,21] Assuming that the Poisson's ratio is constant over the temperature range concerned and using the relation among the shear modulus G, Young's modulus E and Poisson's ratio ν, given by $G (=E/2(1+\nu))$, the shear modulus of the composite was given by $G_c = 144 - 0.0129T$.

It has been shown that the relation of the strain rate $\dot{\varepsilon}$ to the flow stress σ in plastic deformation of the Al_2O_3/YAG composite at around 1700–2023 K is expressed by:[6,7,12,15]

$$\dot{\varepsilon} = A\sigma^n \exp\left(-\frac{Q}{RT}\right) \quad (3)$$

where A is the constant, n is the stress exponent, Q is the activation energy for plastic deformation and R is the gas constant. Waku et al.[12] found $n = 5$–6 and $Q = 670$–905 kJ/mol from the compressive creep test and Yoshida et al.[15] found $n = 6$ and $Q = 730$ kJ/mol from the static compressive test of the present composite.

It has been known that the plastic and creep deformation of ceramics is controlled by dislocation mechanisms (dislocation glide and climb, dissolution of dislocation loops and so on) or boundary mechanisms (sliding accommodated by diffusion, sliding with glassy phase at grain boundary, and so on), as summarized by Cannon and Langdon[30] and Davidge.[31] The boundary mechanisms are not the present case since the present composite has very clean interface between Al_2O_3 and YAG and has no grain boundary and no glassy phase.[6,8,11] Waku et al.[12] and Yoshida et al.[15] observed the dislocation structures in both Al_2O_3 and YAG in the plastically deformed specimens with the transmission electron microscope. Their observation result, together with the measured value of $n = 5$–6, suggests that the plastic deformation of this composite can be attributed to the dislocation glide and clime, controlled by climb.[30,31]

Concerning the tensile behavior of this composite, the temperature and displacement speed dependence of flow stress is not fully known. In the present work, the A, n and Q values were determined as follows. (i) Based on the dislocation mechanism for plastic deformation as stated above, the n value was taken to be 5. (ii) The A and Q values were estimated from the result of Waku et al.,[11] who reported the stress–strain curves up to 2023 K under a strain rate of $10^{-4}\,s^{-1}$ (corresponding to a displacement speed of 10^{-7} m/s) using the unnocthed specimen whose overall shape and size were same as the present specimens (Fig. 3(a)). As the variation of the flow stress with strain in the plastic region was small in the reported stress–strain curve (Fig. 11 in Ref. 4), the stress–strain curve was approximated to be elastic-perfect plastic. Then, from the fitting of the flow stress-values at 1923–2023 K to Eq. (3) with $n = 5$, Q was estimated to be 750 kJ/mol, which was nearly the same as 670–905 kJ/mol and 730 kJ/mol estimated from the compressive creep and static tests mentioned above. Thus, we had the following σ (MPa)–$\dot{\varepsilon}$ relation:

$$\sigma = \left\{\frac{\dot{\varepsilon}}{1.23 \times 10^5}\right\}^{1/5} \left\{\frac{\exp\{1.81 \times 10^4\}}{T}\right\} \quad (4)$$

The yield stress (and flow stress after yielding) of the composite is a function of strain rate and temperature. In this work, the Von Mises criterion was applied as the criterion for yielding using Eq. (4). In advance to the application of the present finite element analysis to the notched tensile specimens, it was checked, whether the present finite element analysis using Eq. (4) and E_c, ν_c and G_c mentioned above can describe the behavior of the unnotched specimens or not. Fig. 5 shows the comparison of the measured flow stresses with the calculated ones by the finite element analysis. The calculated values are in good agreement with the measured ones.

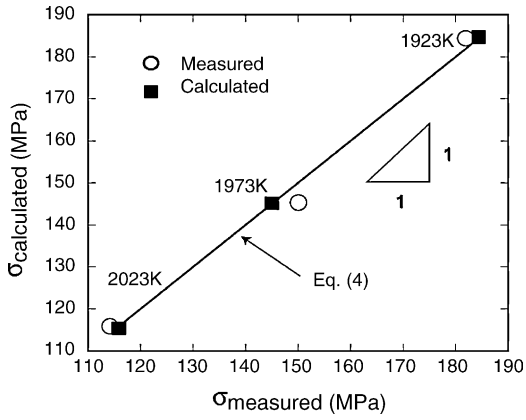

Fig. 5. Comparison of the calculated plastic flow stresses by the finite element method with the measured ones of the unnotched tensile specimens deformed at 1923, 1973 and 2023 K under the displacement speed of 10^{-7} m/s.

3. Results and discussion

3.1. Experimental results of stress–displacement curve and notched strength

Fig. 6 shows the measured tensile stress–displacement curves of the notched specimens at the temperatures of 1873, 1923, 1973 and 2023 K under the given displacement speed of 10^{-7} m/s. The stress is given by the gross stress, estimated by dividing the load by the cross-sectional area. The specimens at the lower temperatures of 1873 and 1923 K fractured in a brittle manner in the elastic range, while those at the higher temperatures of 1973 and 2023 K fractured in a ductile manner, accompanied by the plastic deformation in spite of the existence of the notch. Fig. 7 shows the measured stress–displacement curves of the notched specimens at the displacement speed of 10^{-8}, 10^{-6}, 10^{-6} and 10^{-5} m/s under the given temperature of 2023 K. The specimens fractured in a ductile manner when deformed at the lower displacement–speeds of 10^{-8} and 10^{-7} m/s, while they fractured in a brittle manner when deformed at the higher displacement speeds of 10^{-6} and 10^{-5} m/s. In this way, the fracture mode turned from brittle to ductile with increasing temperature under the given displacement speed (Fig. 6) and with decreasing displacement speed under the given temperature (Fig. 7).

Fig. 8 shows the (a) temperature-dependence of the measured notched strength under the displacement speed of 10^{-7} m/s and (b) displacement speed dependence under the temperature of 2023 K. (a) to (d) in Fig. 8(a) and (b) refer to the specimens whose stress–displacement curves are shown in (a) to (d) in Figs. 6 and 7, respectively. The closed and open circles refer to the specimens that fractured in the brittle and ductile manners, respectively. The apparent fracture toughness K_Q estimated by Eq. (1) of the specimens that fractured in a brittle manner (closed circles) is also presented. Following features are read.

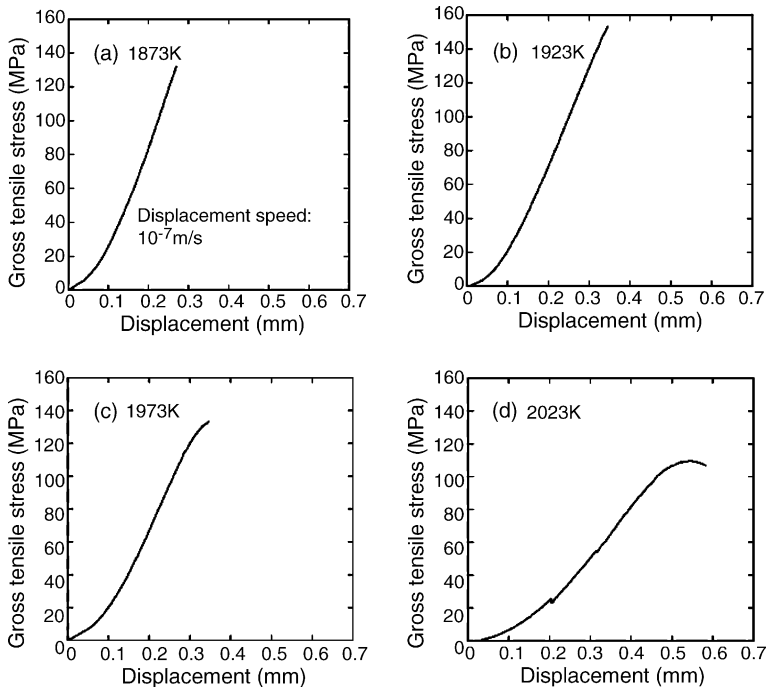

Fig. 6. Measured gross tensile stress–displacement curves of the notched specimens tested at the temperatures of (a) 1873 K, (b) 1923 K, (c) 1973 K and (d) 2023 K under the displacement speed of 10^{-7} m/s.

(1) The notched strength at the displacement speed of 10^{-7} m/s increases, reaching maximum at 1923 K, and then decreases with increasing temperature (Fig. 8(a)). Also, the notched strength at 2023 K increases, reaching maximum at the displacement–speed of 10^{-6} m/s and then decreases with increasing displacement speed (Fig. 8(b)). In this way, the expected temperature and displacement speed dependence of the notched strength

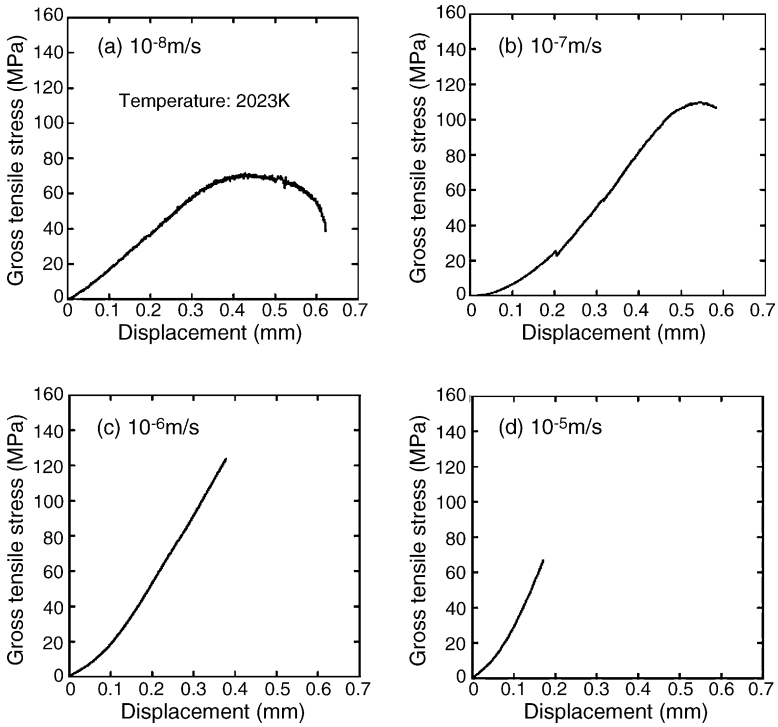

Fig. 7. Measured gross tensile stress–displacement curves of the notched specimens deformed at the displacement speeds of (a) 10^{-8} m/s, (b) 10^{-7} m/s, (c) 10^{-6} m/s and (d) 10^{-5} m/s under the temperature of 2023 K.

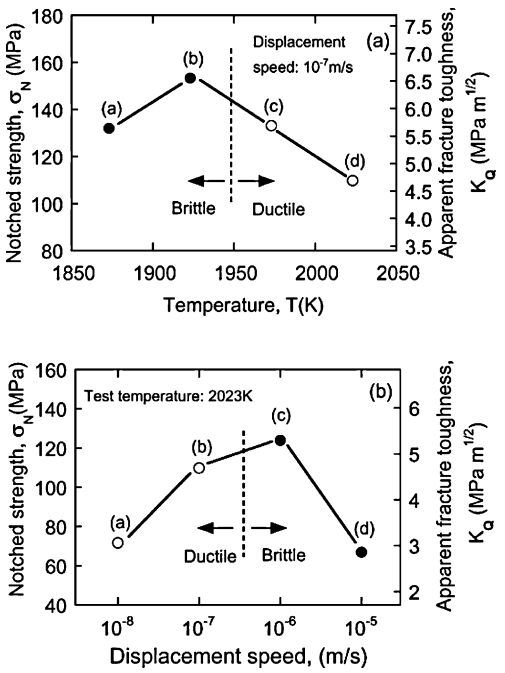

Fig. 8. Measured notched strength σ_N plotted against (a) temperature and (b) displacement speed. The open (◯) and closed (●) circles refer to the ductile and brittle fracture modes, respectively. The right axis shows the apparent fracture toughness K_Q, which was estimated for the specimens fractured in brittle mode. (a) to (d) attached to the data points in (a) and (b) refer to the specimens whose stress–displacement curves are presented in Figs. 6 and 7.

((i) and (ii) mentioned in Section 1) are actually observed.

(2) In our former work,[21] the apparent mode I fracture toughness, K_Q, measured by the bending test was around 2.5–8 MPa $(m)^{1/2}$ in the temperature range of room temperature to 2023 K, depending on the test temperature and displacement speed (Fig. 2). The measured values of K_Q of the present work are 2.8–6.2 MPa $(m)^{1/2}$, being nearly the same as the former values.

(3) The fracture mode of the notched tensile specimens turns from brittle to ductile when the temperature becomes high under the given displacement speed (Figs. 6 and 8(a)) and it turns from ductile to brittle when the displacement speed becomes high under the given temperature (Figs. 7 and 8(b)). In spite of the existence of the notch, the temperature and displacement speed dependence of the brittle–ductile transition shows the same tendency as that of the unnotched bending specimens (Fig. 1).

3.2. Finite element analysis

The features mentioned above suggest that the stress state at the notch tip plays a dominant role to determine the fracture behavior and notched strength of the composite through the temperature and displacement speed dependence of the plastic flow stress.

When the temperature is low or the displacement speed is high, the size of the plastic zone ahead of the notch tip is small due to the high flow stress, which allows the extension of the notch, resulting in brittle fracture. The plastic zone size increases with increasing temperature (with decreasing displacement speed), which acts to raise fracture toughness. The feature in the present results that the notched strength increases with increasing temperature (decreasing displacement speed) within the range of brittle fracture (closed circles in Fig. 8(a) and (b)) can be attributed to such an effect.

On the contrary, when the temperature is high or the displacement speed is low, the flow stress is low, which allows the overall yielding of the ligament, resulting in ductile fracture. In this ductile fracture process, the decrease in flow stress with increasing temperature (with decreasing displacement speed) acts to reduce the stress carrying capacity of the ligament. The feature in the present results that the notched strength decreases with increasing temperature (decreasing displacement speed) within the range of ductile fracture (open circles in Fig. 8(a) and (b)) can be attributed to such an effect.

Whether such a behavior surely occurred or not in the present specimens was examined by the finite element analysis. Figs. 9 and 10 show the calculated distribution of the plastic zone and equivalent stress at the measured fracture stress of the composite, respectively. The plastic zone and equivalent stress at the test temperatures 1873, 1923, 1973

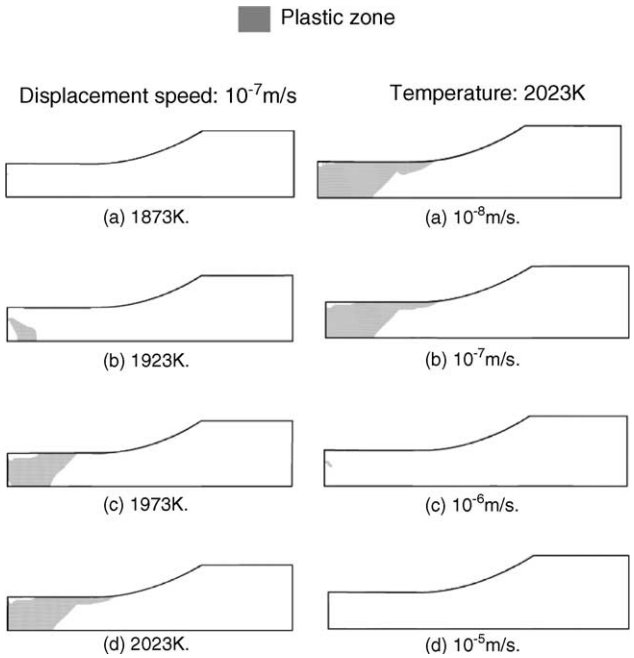

Fig. 9. Distribution of plastic zone in the notched specimens at the experimentally measured fracture stress, calculated by the finite element analysis. The calculation result for the specimens deformed at the temperatures of (a) 1873 K, (b) 1923 K, (c) 1973 K and (d) 2023 K under the displacement speed of 10^{-7} m/s are presented in the left hand side, and those for the specimens deformed at the displacement speeds of (a) 10^{-8} m/s, (b) 10^{-7} m/s, (c) 10^{-6} m/s and (d) 10^{-5} m/s under the temperature of 2023 K are presented in the right hand side.

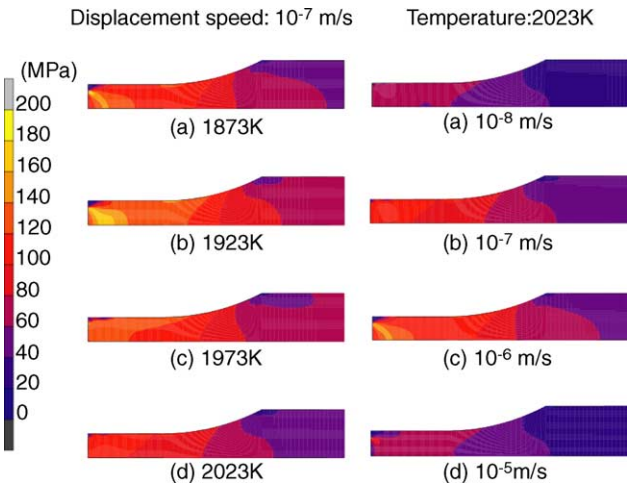

Fig. 10. Distribution of the equivalent stress in the notched specimens at the experimentally measured fracture stress, calculated by the finite element analysis.

and 2023 K under the displacement speed 10^{-7} m/s are presented in the left hand side in Figs. 9 and 10, and those at the displacement speeds 10^{-8}, 10^{-7}, 10^{-6} and 10^{-8} m/s under the temperature 2023 K are presented in the right hand side. The plastic zone is shown by the gray color.

Evidently, the plastic zone size increases and decreases with increasing temperature and displacement speed, respectively. In the specimens that fractured in a brittle manner at the temperatures of 1873 and 1923 K and at the displacement speeds of 10^{-6} and 10^{-5} m/s, the plastic zone is small (Fig. 9) and the stress concentration at the notch tip is high (Fig. 10), while in the specimens that fractured in a ductile manner at the temperatures of 1973 and 2023 K and at the displacement speeds of 10^{-8} and 10^{-7} m/s, the plastic zone covers the ligament portion (Fig. 9) and the stress is nearly uniform in such a portion (Fig. 10). These results show that the feature, "the notched strength increases with increasing temperature (decreasing displacement speed) in the region of brittle fracture (closed circles in Fig. 8(a) and (b))", can be accounted for well by the increase in plastic zone size with increasing temperature (with decreasing displacement speed). Also the feature, "the notched strength decreases with increasing temperature (decreasing displacement speed) in the region of ductile fracture (open circles in Fig. 8(a) and (b))", can be accounted for well by the overall plastic deformation of the ligament portion.

It is noted here that the present composite behave like a metal. Once plastic deformation takes place at ultra high temperatures. Such a feature is important for safety design in application.

4. Conclusions

The fracture behavior of the Al_2O_3/YAG eutectic composite was investigated by tensile test at ultra high temperatures 1873 to 2023 K using notched specimens under the displacement speed of 10^{-8} to 10^{-5} m/s, and the results were analyzed by the finite element method. Main results are summarized as follows:

(1) The dependences of the notched strength on temperature and displacement speed had the following features. (a) The notched strength under the given displacement speed of 10^{-7} m/s increased, reaching maximum at 1923 K, and then decreased with increasing temperature. The specimens fractured in the brittle manner at 1873 and 1923 K and in the ductile manner at 1973 and 2023 K. (b) The notched strength under the given temperature of 2023 K increased, reaching maximum at the displacement speed of 10^{-6} m/s, and then decreased with increasing displacement speed. The specimens fractured in the ductile manner at the displacement speeds of 10^{-8} and 10^{-7} m/s and in the brittle manner at the speeds of 10^{-5} and 10^{-6} m/s.

(2) The distribution of the plastic zone and the equivalent stress was calculated by the finite element method. The feature (a) in (1) was accounted for by the increase in plastic zone size ahead of the notch with increasing temperature in the relatively lower temperature region (1873 and 1923 K) and by the decrease in stress carrying capacity of the fully yielded ligament with increasing temperature in the relatively higher temperature region (1973 and 2023 K). The feature (b) was accounted for by the increase in stress carrying capacity of the fully yielded ligament with increasing displacement speed in the relatively lower displacement speed region (10^{-5} and 10^{-6} m/s) and by the decrease in plastic zone size ahead of the notch with increasing displacement in the relatively higher displacement speed region (10^{-7} and 10^{-8} m/s).

Acknowledgments

The authors wish to express their gratitude to Japan Ultra High Temperature Materials Research Center, Gifu and Yamaguchi, and to Asian Office of Aerospace Research and Development, Tokyo, for the support.

References

1. Sorrell, C. C., Beratan, H. R., Brad, R. C. and Stubican, V. S., Directional solidification of (Ti, Zr) carbide-(Ti, Zr) diboride eutectics. *J. Am. Ceram. Soc.*, 1984, **67**, 190–194.
2. Sorrell, C. C., Stubican, V. S. and Bradt, R. C., Mechanical-properties of ZrC–ZrB_2 and ZrC–TiB_2 directionally solidified eutectics. *J. Am. Ceram. Soc.*, 1986, **69**, 317–321.
3. Mazerolles, L., Michel, D. and Portier, R., Microstructure and mechanical-behavior of Al_2O_3–$ZrO_2(Y_2O_3)$. *J. Phys.*, 1986, **47**(C-1), 335–339.
4. Mazerolles, L., Michel, D. and Portier, R., Interfaces in oriented Al_2O_3–ZrO_2 (Y_2O_3) eutectics. *J. Am. Ceram. Soc.*, 1986, **69**, 252–255.

5. Echigoya, J., Takabayashi, Y., Suto, H. and Ishigame, M., Structure and crystallography of directionally solidified Al_2O_3–ZrO_2–Y_2O_3 eutectic by the floating zone-melting method. *J. Mater. Sci. Lett.*, 1986, **5**, 150–152.
6. Waku, Y., Nakagawa, N., Otsubo, H., Ohsora, Y. and Kohtoku, Y., High temperature properties of unidirectionally solidified Al_2O_3/YAG composites. *J. Jpn. Inst. Metals*, 1995, **59**, 71–78.
7. Waku, Y., Nakagawa, N., Wakamoto, T., Otsubo, H., Shimizu, K. and Kohtoku, Y., Excellent high-temperature properties of YAG matrix composites reinforced with sapphire phases. In *Processing and Fabrication of Advanced Materials IV*, ed. T. S. Srivatsan and J. J. Moore. The Minerals, Metals and Materials Society, Warrendale, PA, 1996, pp. 323–339.
8. Waku, Y., Otsubo, H., Nakagawa, N. and Kohtoku, Y., Sapphire matrix composites reinforced with single crystal YAG phases. *J. Mater. Sci.*, 1996, **31**, 4663–4670.
9. Yang, J. M., Jeng, S. M. and Chang, S. Y., Fracture behavior of directionally solidified $Y_3Al_{15}O_{12}$/Al_2O_3 eutectic fiber. *J. Am. Ceram. Soc.*, 1996, **79**, 1218–1222.
10. Waku, Y., Nakagawa, N., Otsubo, H., Shimizu, K. and Kohtoku, Y., A ductile ceramic eutectic composite with high strength at 1873 K. *Nature*, 1997, **389**, 49–52.
11. Waku, Y., Nakagawa, N., Wakamoto, T., Otsubo, H., Shimizu, K. and Kohtoku, Y., High temperature strength and thermal stability of unidirectionally solidified Al_2O_3/YAG eutectic composite. *J. Mater. Sci.*, 1998, **33**, 1217–1224.
12. Waku, Y., Nakagawa, N., Wakamoto, T., Otsubo, H., Shimizu, K. and Kohtoku, Y., The creep and thermal stability characteristics of a unidirectionally solidified Al_2O_3/YAG eutectic composite. *J. Mater. Sci.*, 1998, **33**, 4843–4951.
13. Matson, L. E. and Hecht, N., Microstructural stability and mechanical properties of directionally solidified alumina/YAG eutectic monofilaments. *J. Europ. Ceram. Soc.*, 1999, **19**, 2487–2501.
14. Brewer, L. N., Endler, D. P., Austin, S., Dravid, V. P. and Collins, J. M., Interface modification for increased fracture toughness in reaction-formed yttrium aluminum garnet/alumina eutectic composites. *J. Mater. Res.*, 1999, **14**, 3907–3912.
15. Yoshida, H., Shimura, K., Suginohara, S., Ikuhara, Y., Sakuma, T., Nakagawa, N. *et al.*, High-temperature deformation in unidirectionally solidified eutectic Al_2O_3–YAG single crystal. *Key Eng. Mater.*, 2000, **171–174**, 855–862.
16. Nakagawa, N., Waku, Y., Wakamoto, T., Otsubo, H., Shimizu, K. and Kohtoku, Y., High temperature properties and thermal stability of a unidirectionally solidified Al_2O_3/$Er_3Al_5O_{12}$ eutectic composite. *J. Jpn. Inst. Metals*, 2000, **64**, 101–107.
17. Echigoya, J., Hayashi, S. and Obi, Y., Directional solidification and interface structure of $BaTiO_3$–$CoFe_2O_4$ eutectic. *J. Mater. Sci.*, 2000, **35**, 5587–5591.
18. Orera, V. M., Merino, R. I., Pardo, J. A., Larrea, A., Pena, J. I., Gonalez, C. *et al.*, Microstructure and physical properties of some oxide eutectic composites processed by directional solidification. *Acta Mater.*, 2000, **48**, 4683–4689.
19. Pastor, J. Y., Poza, P., Llorca, J., Pena, J. I., Merino, R. I. and Orera, V. M., Mechanical properties of directionally solidified Al_2O_3–$ZrO_2(Y_2O_3)$ eutectics. *Mater. Sci. Eng. A*, 2001, **308**, 241–249.
20. Sayir, A. and Farmer, S. C., The effect of the microstructure on mechanical properties of directionally solidified Al_2O_3/$ZrO_2(Y_2O_3)$ eutectic. *Acta Mater.*, 2000, **48**, 4691–4697.
21. Ochiai, S., Ueda, T., Sato, K., Hojo, M., Waku, Y., Nakagawa, N. *et al.*, Deformation and fracture behavior of Al_2O_3/YAG composite from room temperature to 2023 K. *Compos. Sci. Technol.*, 2001, **61**, 2117–2128.
22. Frazer, C. S., Dickey, E. C. and Sayir, A., Crystallographic texture and orientation variants in Al_2O_3–$Y_3Al_5O_{12}$ directionally solidified eutectic crystals. *J. Crystal Growth*, 2001, **233**, 187–195.
23. Harlan, N. R., Merino, R. I., Pena, J. I., Larrea, A., Orera, V. M., Gonzalez, C. *et al.*, Phase distribution and residual stresses in melt-grown Al_2O_3–$ZrO_2(Y_2O_3)$ eutectics. *J. Am. Ceram. Soc.*, 2002, **85**, 2025–2032.
24. Brewer, L. N., Dravid, V. P., Dhalenne, G. and Velazquez, M., Solid-solution directionally solidified oxide composites: Part I. Eutectic growth and characterization. *J. Mater. Res.*, 2002, **17**, 760–767.
25. Andreeta, E. R. M., Andreeta, M. R. B. and Hernades, A. C., Laser heated pedestal growth of Al_2O_3/$GdAlO_3$ eutectic fibers. *J. Crystal Growth*, 2002, **234**, 782–785.
26. Fernandez, J. M., Sayir, A. and Farmer, S. C., High temperature creep deformation of directionally solidified Al_2O_3/$Er_3Al_5O_{12}$. *Acta Mater.*, 2003, **51**, 1705–1720.
27. Okamura, H., *Introduction to Linear Elastic Fracture Mechanics*. Baifu-kan, Tokyo, 1975, pp. 216–222 (in Japanese).
28. Ochiai, S., Ueda, T., Sato, K., Hojo, M., Waku, Y., Sakata, S. *et al.* Elastic modulus and coefficient of thermal expansion of Al_2O_3/YAG composite at ultra high temperatures. *Mater. Sci. Res. Int. Special Technical Publication*-2, Mater. Sci. Res. Int., Kyoto, 2001, pp. 281–285.
29. Waynant, R. and Ediger, M., *Electro-optics Handbook*. Mcgraw-Hill Inc., New York, 1994, pp. 11.13–11.23.
30. Cannon, W. R. and Lagdon, T. G., Review: creep of ceramics. *J. Mater. Sci.*, 1983, **18**, 1–50.
31. Davidge, R. W., *Mechanical Behavior of Ceramics*. Cambridge University Press, 1979, pp. 64–74.